11-10-2020

Cost Minimization of Battery-Supercapacitor Hybrid Energy Storage for Hourly Dispatching Wind-Solar Hybrid Power System

Pranoy Roy
University of Kentucky, pranoyroy@uky.edu

Jiangbiao He
University of Kentucky, Jiangbiao.He@uky.edu

Yuan Liao
University of Kentucky, yuan.liao@uky.edu

Cost Minimization of Battery-Supercapacitor Hybrid Energy Storage for Hourly Dispatching Wind-Solar Hybrid Power System

Digital Object Identifier (DOI)
https://doi.org/10.1109/ACCESS.2020.3037149

Notes/Citation Information
Published in *IEEE Access*, v. 8.

IEEE Access
Multidisciplinary | Rapid Review | Open Access Journal

Received September 29, 2020, accepted October 28, 2020, date of publication November 10, 2020,
date of current version December 7, 2020.

Digital Object Identifier 10.1109/ACCESS.2020.3037149

Cost Minimization of Battery-Supercapacitor Hybrid Energy Storage for Hourly Dispatching Wind-Solar Hybrid Power System

PRANOY ROY, (Graduate Student Member, IEEE), JIANGBIAO HE, (Senior Member, IEEE), AND YUAN LIAO, (Senior Member, IEEE)
Department of Electrical and Computer Engineering, University of Kentucky, Lexington, KY 40506, USA
Corresponding author: Jiangbiao He (jiangbiao@ieee.org)

ABSTRACT This study demonstrates a dispatching scheme of wind-solar hybrid power system (WSHPS) for a one-hour dispatching period for an entire day utilizing battery and supercapacitor hybrid energy storage subsystem (HESS). A frequency management approach is deployed to extend the longevity of the batteries through extensively utilizing the high energy density property of batteries and the high power density property of supercapacitors in the HESS framework. A low-pass filter (LPF) is employed to decouple the power between a battery and a supercapacitor (SC). The cost optimization of the HESS is computed based on the time constant of the LPF through extensive simulations in MATLAB/SIMULINK platform. The curve fitting and Particle Swarm Optimization approaches are applied to seek the optimum value of the LPF time constant. Several control algorithms as a function of the battery state of charge are developed to achieve accurate estimation of the grid reference power for each one-hour dispatching period. This estimation helps to minimize the energy storage cost, in addition to ensuring that the HESS has sufficient capacity for next-day operation. The optimum value of depth of discharge for HESS considering both cycling and calendar expenses has also been investigated for the best competitive energy storage cost for hourly dispatching the power of the WSHPS. This research also presents an economic comparison to investigate the significance of using different types of energy storage for hourly dispatching the WSHPS. The simulation results show that the presented HESS is superior to battery or SC-only operation.

INDEX TERMS Battery, cost analysis, hourly dispatching, hybrid energy storage, hybrid wind-solar power system, particle swarm optimization, supercapacitor.

I. INTRODUCTION

Renewable energy resources have witnessed explosive growth globally over the past decade. For instance, renewable energy sources provided approximately 17% of total U.S. electricity generation in 2019. According to the U.S. Energy Information Administration (EIA), this increasing trend of renewable energy consumption will continue through 2050 [1]. With strong government incentives and encouragement of green energy utilization, renewable energy sources, particularly Photovoltaic (PV) and Wind Turbine (WT) have become the most attractive power generation solutions. As a consequence, the global penetration of the PV and WT energy in power systems have been substantially increasing. From 2017 to 2018, the WT installed capacity expanded from 540 GW to 591 GW, and the solar PV installed capacity expanded from 405 GW to 505 GW [2]. As the output of the PV and WT substantially relies on climate conditions, i.e., clouds movement and wind speed, their output power exhibits unstable attributes. Consequently, substantial penetration of these types of intermittent renewable energy sources into the utility grid poses severe technical challenges on power quality, generation dispatch control, and grid reliability. Therefore, renewable energy plant operators will be pressured to provide a constant power dispatch, in a manner like what has been provided by the conventional fossil fuel power plants.

As more PV and WT are connected to the grid, overgeneration and curtailment become the rising concerns for the grid operators. There are primarily two causes, namely,

The associate editor coordinating the review of this manuscript and approving it for publication was Eklas Hossain.

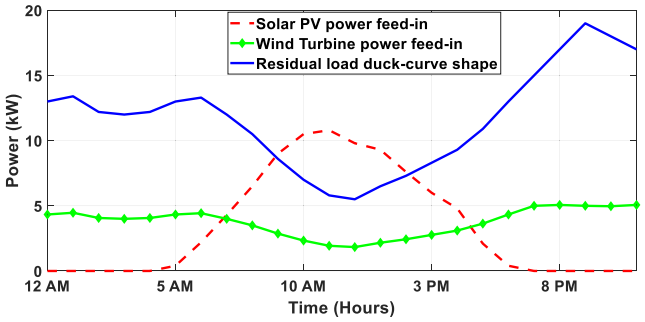

FIGURE 1. Duck curve illustration.

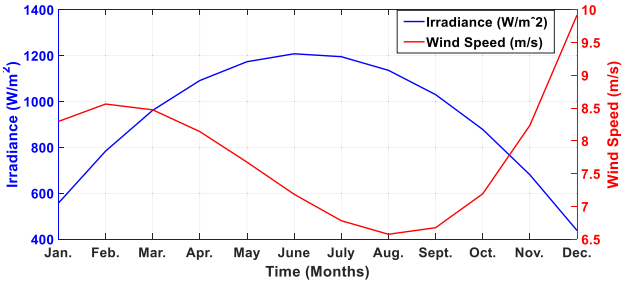

FIGURE 2. PV and WT complementary profiles illustration.

TABLE 1. Battery and SC performance comparison.

Properties	Battery	Supercapacitor
Specific energy density	10-100 Wh/kg	1-10 Wh/kg
Specific power density	<1000 W/kg	<10,000 W/kg
Cycle life	1000	>500,000
Charge/discharge efficiency	70-80 %	85-98 %
Fast charge time	1-5 hr	0.3-30 sec
Discharge time	0.3-3 hr	0.3-0.30 sec

local transmission constraints and supply-wide oversupply for renewable energy curtailment. The range of the curtailment levels between 1% to 4% of wind generation has occurred, but higher levels of curtailment have also been reported [3]. Negative pricing and renewable energy generation curtailment take place when the inflexible traditional generator, like nuclear and coal plants, cannot be employed to generate lower power. Fig. 1 illustrates the duck curve that can be utilized to demonstrate the significant challenge of accommodating solar and wind energy, and the probability for overgeneration and curtailment.

It is well known that either wind or solar source cannot provide a continuous power supply to the load individually. It is also noted that the peak operating time for wind and solar system occur at different times of the day and the year. In fact, solar and wind energy resources are complementary to each other, due to the weather and climate patterns. As a consequence, the energy production by Wind-PV resources offset each other on a seasonal or day-to-day basis. For instance, the monthly average solar irradiance and wind speed of the Colorado state in 2019 is shown in Fig. 2 [4]. Therefore, the hybrid utilization of the PV and WT deserves more attention because they have the advantages of complementary power profiles. Hybridization techniques can be developed to solve the variable nature of solar and wind power.

The wind-solar hybrid power system (WSHPS) incorporates the PV and WT subsystems together to provide increased systematic efficiency, lower required capacity of energy storage, and improved stability in power supply [5]. The WSHPS can compensate the undesired intermittent variations with a single renewable energy source, which is more beneficial than employing an individual PV or wind turbine system in weak utilities. Furthermore, the WSHPS has the ability to minimize the infrastructure expenses, especially for rural electrification projects, by assisting the point of generation and consumption being adjoined to each other. Hence, the WSHPS schemes at a single location are emerging as a primary tendency in the global transformation to renewable energy. For example, the NextEra energy resources is going to construct the largest hybrid renewable project in the USA, a 700 MW facility that consists of 250 MW WT, 250 MW PV, and 200 MW Energy storage in Oklahoma [6].

The uncertainty of renewable energy resources can be reduced further by including the energy storage system (ESS) in the WSHPS framework. Specifically, the ESS facilitates ancillary services such as frequency stability, peak regulation, harmonic reduction, voltage fluctuation and flicker mitigation, transient stability, and load leveling. Batteries and Supercapacitors (SC) are frequently utilized among several types of ESS available in the market. Examples of practical utility-scale ESS include the 32 MW Li-ion battery installed in a 98 MW wind farm by AES in Elkins, West Virginia, the 8 MW, and the 32 MWh Li-ion battery installed in the Tehachapi energy storage project in California [7], [8]. Table 1 shows the relative properties of the battery and SC [9]. The conventional capacitor also exhibits similar characteristics to the SC except that its size is much larger and its lifetime is only half that of the SC [10].

Ref [9] shows that the battery energy storage system (BESS) has a high energy density property, but a low-power ramp rate that signifies the BESS charging-discharging rates are not fast enough to meet the peak or pulse load demand. However, the supercapacitors energy storage system (SESS) has a high power ramp rate, but low energy density property. Consequently, the SC cannot maintain the load demand for an expected duration. It is evident that none of these two ESS has both the properties of high power density and high energy density. Hence, there is a possibility to incur high installation expense if only one type of ESS is deployed to meet both the power and energy capacity specifications. Accordingly, a hybrid energy storage system (HESS) consisting of a BESS and a SESS can be leveraged to develop a cost-effective ESS, where the SC facilitates to alleviate the fast-changing power components passing through the battery, which is beneficial for increasing the battery's service life [11].

There are several challenges existing for the high penetration of intermittent renewable energy into the utility, such as voltage and frequency regulation, mismatch between generated power and load demand, grid operation economics, and scheduling of generation units. Hence, grid operators need to take additional actions to maintain system stability. For instance, fossil-fueled generators must be turned on and off or adjust their outputs more periodically to accommodate the power variations due to the presence of additional solar and wind power into the grids. This type of cycling of fossil-fueled generators is responsible for increasing its wear and tear costs and decreasing its efficiency as well. The high penetrations of solar power lead to cycling costs of \$0.47/MWh to \$1.28/MWh per fossil-fueled generator, which was reported in [12]. Therefore, a constant power dispatch commitment at an acceptable interval is demanded from the WSHPS framework to overcome the aforementioned economic challenges.

A. OBJECTIVES AND CONTRIBUTIONS

The main objective of this study is to enhance the integration of renewable energy that secures a desired hourly dispatching of the WSHPS output power at one-hour increments for an entire day to the power grid. Here, a HESS consisting of the lithium-ion batteries and SC is incorporated into the WSHPS architecture that can accumulate the harvested WSHPS energy and convert the sporadic energy into a dispatchable supply at an intended confidence level.

In this research, it is important to mention that a dispatching scheme is deployed rather than the traditional peak shaving or smoothing approach to provide the WSHPS output power to the utility grid. The dispatching scheme enables the WSHPS to be a reliable source of power for the utility, which can be regulated like any other conventional generators, i.e., thermal and hydropower plants. Furthermore, the WSHPS output power supplied to the grid using a dispatched scheme provides considerable flexibility to the utility grid, especially in the scheduling of generation units, grid operation economics, and grid ancillary services. Since most of the supply side adjustment in the utility grid takes place on an hour-to-hour basis, an one-hour dispatching interval is taken into account in this study.

Here, a low pass filter (LPF) is employed to decouple the HESS power into two different categories: one has a fast-dynamic response specified to the SC while the other has a slow dynamic response specified to the battery. This technique assists the battery in avoiding the fast-changing charging-discharging cycles and a considerable magnitude of discharge current, accordingly prolonging the battery's lifetime. The battery lifetime comparison with and without the SC in the ESS architecture is also explored in this work. Furthermore, curve fitting and Particle Swarm Optimization (PSO) approaches are applied to seek the optimum value of the LPF time constant that yields the most cost-effective HESS for hourly dispatching the WSHPS power scheme. The objective function is minimizing the expenditure of the HESS with the constraint of regulating the SOC of the ESS within a specified range and successfully fulfilling the power demand for each dispatching period.

Besides, several control algorithms based on the battery state of charge (SOC) are developed to achieve accurate estimation of the grid reference power ($P_{Grid,ref}$) for each one-hour dispatching period. The SOC control algorithms also ensure the ESS to complete each dispatching period with the same SOC as it started. This mechanism plays a significant role in regulating the battery SOC within a specified range which helps to minimize the energy storage cost and ensures that the ESS has enough capacity available for next-day operation. An economic comparison is presented to investigate the impact of using different types of SOC control algorithms in the $P_{Grid,ref}$ estimation.

In this research, the $P_{Grid,ref}$ for the WSHPS is generated utilizing two different schemes, i.e., (i) dispatchable power reference case—estimating the $P_{Grid,ref}$ utilizing the methodology described later in this paper and (ii) load following case—load profile for 2.5 MW utility is collected from CAISO and is utilized as a $P_{Grid,ref}$ for the entire system. A comparative economic assessment between the two schemes is also investigated in this study.

The expenditure associated with the ESS substantially depends on two aspects, namely, (i) lifetime of the ESS and (ii) minimum capacity required of the ESS. The service life of the ESS primarily relies on the utilization of DOD and the rate of charging-discharging power changes. In general, the ESS manufacturers specify energy storage cycle life as a function of DOD, and the deeper discharge of the ESS reduces the lifetime as well as increases its expense substantially. Hence, the SOC of the ESS has always been controlled to prevent the ESS depletion beyond its recommended DOD. This kind of constraint facilitates to prolong the lifespan of the ESS significantly. However, such SOC regulation is responsible for restricting the full utilization of the ESS, which is one contributing factor extending the required energy storage capacity. Thus, based on the usage of SOC, there is a trade-off between the service life and the minimum capacity required of the ESS. In this research, the optimum value of DOD has been investigated which exhibits the best competitive ESS cost for hourly dispatching the WSHPS power to the utility grid. In addition, after seeking the optimal value of DOD for the ESS, one secondary SOC control algorithm is also employed to regulate the ESS SOC in the optimal range.

The objective here is to develop a cost-effective ESS for the hourly dispatch of WSHPS power. An economic comparison is presented to investigate the impact of using three different types of energy storage systems: (i) battery only, (ii) HESS framework, i.e., the combination of a Li-ion battery and a SC, and (iii) SC only. Also, an economic comparison of using three different types of renewable energy sources—(i) PV only, (ii) WSHPS framework, i.e., the combination of the WT and the PV, and (iii) WT only, with HESS framework for the fulfillment of the $P_{Grid,ref}$ is analyzed in this research. To obtain annual energy storage costs, the actual PV

and WT data of four different days as representative of four seasons, which was recorded by U.S. National Renewable Energy Laboratory (NREL), is used in this research [13].

To exhibit the effectiveness of the proposed HESS control framework, a one-hour simulation is illustrated considering all possible cases of the availability of sources investigated in this study—(i) PV+WT+ESS, (ii) WT+ESS, (iii) PV+ESS, and (iv) ESS only, to dispatch the desired $P_{Grid,ref}$ for the entire duration.

The rest of this paper is organized as follows: Section II presents the state-of-the-art review on this same topic. Section III describes the proposed methodology for hourly dispatching the WSHPS power. Section IV verifies the effectiveness of the proposed methodology and control methods through simulations. Finally, the conclusions of this research are drawn in Section V.

II. STATE-OF-THE-ART REVIEW

Various strategies have been contemplated in the literature to enable the PV and WT power to be dispatchable by deploying different types of ESS and control techniques. In [14], [15], a control technique has been proposed to smooth the output of the renewable energy sources where the battery has been dispatched on an hourly basis. An iterative procedure has been utilized to calculate the required size of the battery. The control strategy is employed to maintain certain SOC of the battery in order to extend its lifetime. Therefore, a larger size of the battery is required to have an effective hourly dispatch. Another improved control approach for a grid-connected PV and battery energy system has been investigated in [16] to dispatch the PV power smoothly on an hourly basis to the utility grid. However, these control techniques do not take into account the daily cycling of the battery. Furthermore, the battery has been highly exposed to fast-changing components of intermittent PV power that would cause significant downtime cost once the battery fails. Consequently, these proposed techniques might not be feasible to develop cost-effective energy storage for hourly dispatching the PV power.

Wang *et al.* attempted to develop a BESS in a buffer scheme to attenuate the effects of unsteady input power from wind farms [17]. A computational procedure has been utilized to determine the BESS capacity that ensures a constant dispatched power from the wind farm to the connected grid. The power dispatched in a day was set to be a constant level while the optimal BESS capacity has been investigated. It has been found that the wind farm achieved a substantial profit at the optimal BESS capacity. Since the control strategy utilized in this study depends on the day that the wind was studied, the designed BESS capacity may not be unique.

The authors in [18] investigated a min-max renewable energy dispatching approach where the dispatched power was set to the minimum available renewable energy power during the battery charging phase. On the other hand, when the battery switches to the discharging phase, the dispatched power was set to the maximum available renewable power. The complexity of the technique and the large-scale battery rating compared with other dispatching methods might be the downsides of this min-max dispatching method.

In [19], one modified min-max power dispatching method has been proposed to determine the optimal BESS capacity in order to effectively integrate the wind power into the grid. A short-term power dispatch control algorithm has been utilized to smooth the transient power between two consecutive dispatching intervals. Moreover, the battery SOC has been regulated within a safe range utilizing this proposed control algorithm. Since the battery is the only ESS media employed to smooth the wind farm transient power, the charging-discharging cycles of the battery would be extremely high. Therefore, the overall economics of the system might lead to an unacceptable level.

A dual-battery scheme is proposed in [20] to enable a short-term dispatch commitment from the wind power station. In this framework, while the first battery is being charged by the generated wind power, the second battery power is being discharged to the utility grid. The function of the two batteries is shifted when the battery reaches its specified SOC or discharge limit. However, this approach demands the switch-over of battery modules, usually once every few hours, and additional arrangement to diminish the switch-over impact on the utility grid.

In [21], a statistical approach has been utilized to develop a dual-battery scheme in order to dispatch a controllable level of power from a wind power generating station. The expected BESS charging time dictates the scheduled constant discharge power from the BESS to the grid. In this scheme, the BESS is committed to accumulating all the electrical power generated by the wind turbine, therefore, a large-scale battery is required to dispatch a steady power from an intermittent wind power generating station to the grid. Since the cost associated with the BESS is directly proportional to the size of the BESS, the resulting large-scale battery requirements make the system economically unfeasible.

Another HESS framework for the least-cost analysis to realize dispatchable wind power was discussed by Wee *et al.* [22]. A statistical approach is proposed to design a HESS for a wind farm to achieve a firm power dispatch objective while maximizing the wind energy harnessed without modeling power converters. Moreover, the power capacities of the battery and SC were limited in the HESS scheme to become economically viable. Therefore, the rated battery and SC power capacities utilized in this study cannot meet all the possible charging-discharging power requirements. Ref [23] presented a hybrid energy storage system consisting of a lead-acid battery and a SC to absorb or produce the necessary level of power so that constant power can be dispatched to the utility from PV generation. However, the average output power from the PV array might be overestimated.

In [24], various HESS frameworks are investigated to develop a cost-effective ESS for hourly dispatching solar power. Due to various assumptions, the annual cost of the required energy storage may be overestimated or

underestimated. In [25], a low-cost ESS was proposed by evaluating reference generation algorithms for hourly dispatching solar power for 1 MW grid-connected PV arrays. The ambient temperature and PV cell temperature are assumed to be the same during annual energy storage cost calculation and this assumption might affect the estimation accuracy. Another HESS is described in [26] for dispatching solar power for grid-connected PV arrays, which uses an LPF to allocate the power between a battery and a SC. However, LPF time constants may not be optimal.

It is important to note that none of the above studies investigated the capability of dispatching with the hybrid PV-WT scheme, which will be investigated in this paper.

III. THE PROPOSED WSHPS FRAMEWORK

A. SYSTEM STRUCTURE

The proposed WSHPS architecture that consists of a wind energy system (WES) and a PV energy system (PVES) is illustrated in Fig. 3. The PVES consists of PV arrays rated at 1 MW, a unidirectional DC/DC boost converter, and a maximum power point tracking (MPPT) controller. The WES is comprised of a 1.5 MW direct-drive three-phase permanent magnet synchronous generator (PMSG) coupled to a wind turbine, an AC/DC rectifier, and a pitch angle controller. The HESS is coupled in parallel with the WSHPS, and each of the ESS is connected with a bi-directional DC/DC converter. The WSHPS and HESS are connected in parallel to the DC-link capacitor bank that serves as the DC bus, which is tied to a three-level T-type inverter with high-quality output voltages. In this framework, the WSHPS and HESS are coupled to the DC bus as a current source, so controllable power flow is feasible by controlling the current flow through the power converters [27]. The three-level T-type inverter is utilized due to its high efficiency, low total harmonic distortion (THD), and reduced common-mode voltage. A compact output harmonic filter is also demanded as an interface between the inverter and the grid to meet the grid code. In this research, an LCL filter has been designed for its higher efficiency and better harmonic attenuation.

B. CONTROL OF PVES

The output of the PV array substantially relies on two weather conditions: PV irradiation (W/m^2) and PV cell temperature (°C). This investigation is conducted using the actual solar data recorded by NREL. The PV array provides power to the unidirectional boost converter, whose duty ratio is controlled by an incremental conductance (IC) MPPT to extract the maximum power from the PV array. An IC MPPT is simple and more efficient compared to other approaches, i.e., perturb & observe (P&O), open circuit voltage (OCV), and short circuit current (SCC), which are commonly employed to extract maximum power from the PV systems [28]. Thus, IC MPPT has been extensively utilized even though it can contribute to small oscillations next to the maximum power point while it is tracking power from the PV array.

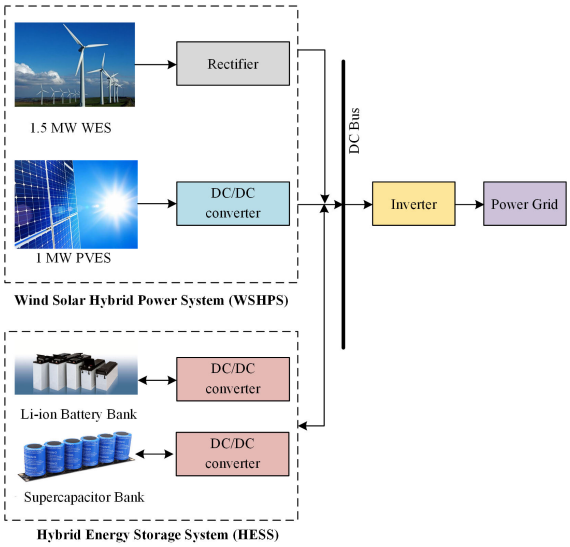

FIGURE 3. Structure of the wind-solar hybrid power system with HESS.

A PV cell is a nonlinear device that can be represented as a current source model. The V-I characteristic equation of a PV cell is shown in (1) and (2) [29].

$$I = I_{sc} - I_d \tag{1}$$

$$I = I_{sc} - I_{os}(e^{\frac{q.(V+I.R_s)}{n.k.T}} - 1) \tag{2}$$

where I_{sc} is the light generated current, I_{os} is the diode reverse saturation current, q is the electronic charge, k is the Boltzmann constant, T is the temperature, V is the terminal voltage of the module, and R_s is the series resistance.

C. PV CELL TEMPERATURE ESTIMATION

In general, the PV cell temperature is higher than the ambient temperature, which unfortunately reduces the PV output power as well as its capacity factor. An effective technique for the PV cell temperature estimation is incorporated in this research [30], as expressed below:

$$(T_m^\circ C) = a \times T_a + b \times I_r - c \times V_w + d \tag{3}$$

where, a, b, c, and d are system-specific regression coefficients, T_a refers to the ambient temperature given in (°C), I_r refers to the solar irradiation given in (W/m^2), and V_w refers to the wind speed given in m/s.

The curve fitting tool is employed to compute the regression coefficients a, b, c, and d [30]. Hence, the PV cell temperature prediction formula can be expressed as:

$$(T_m^\circ C) = 0.943 \times T_a + 0.0195 \times I_r - 1.528 \times V_w + 0.3529 \tag{4}$$

D. CONTROL OF WES

In this study, the implemented WES consists of a WT, PMSG, pitch angle control, drivetrain, and power converter. The PMSG based on WES can associate with the

WT without utilizing a gearbox. The energy conversion in PMSG based on WES takes place through two stages. First, the kinetic energy is captured by the WT blades as mechanical energy. Second, the mechanical energy is transferred through the shaft to PMSG, which converts the mechanical energy to electrical energy. The mechanical output power of a PMSG wind turbine can be expressed as:

$$P_m = \frac{1}{2}\rho A v_w^3 C_p(\lambda, \beta) \tag{5}$$

where P_m is mechanical output power of the turbine (W), ρ is air density (kg/m), A is turbine swept area (m^2), v_w is wind speed (m/s), C_p is the performance coefficient of the turbine, λ is tip speed ratio of the rotor blade tip speed to wind speed and β is blade pitch angle (degree).

The mechanical output power P_m depends significantly on the turbine performance coefficient C_p. In this study, the following generic $C_p(\lambda, \beta)$ model is employed:

$$C_p(\lambda, \beta) = c_1\left(\frac{c_2}{\lambda_i} - c_3\beta - c_4\right)e^{\left(\frac{-c_5}{\lambda_i}\right)} + c_6\lambda \tag{6}$$

$$\frac{1}{\lambda_i} = \frac{1}{\lambda + 0.08\beta} - \frac{0.035}{\beta^3 + 1} \tag{7}$$

where, $c_1 = 0.5176$, $c_2 = 0.116$, $c_3 = 0.4$, $c_4 = 5$, $c_5 = 21$, and $c_6 = 0.0068$. The consequent C_p-λ curve is illustrated in Fig. 4. The C_p-λ curve shows that the maximum value of C_p is achieved for $\beta = 0$ and $\lambda = 8.1$.

When the meteorological data recorded is found at a different height from the WT height, (8) is utilized to calculate the wind speed:

$$V_h = V_{ref}\left(\frac{H}{H_{ref}}\right)^{\alpha} \tag{8}$$

where V_h is the wind speed at turbine height (H), V_{ref} is the wind speed recorded by a meteorological station at height (H_{ref}) and α is the surface roughness factor which is around 1/7 in an open space surface.

E. LI-ION BATTERY DEGRADATION MODEL

To consider calendar aging for the battery usage, a degradation model proposed in [31] is incorporated in this research. The expected lifetime of the battery decreases due to its degradation properties over the period, which can be expressed as:

$$\frac{1}{T_{life}} = \left[\sum_{i=1}^{N}\frac{DOD_i^2}{2N_{cycles}^{ref}} + \frac{T}{T_{calendar}^{ref}}\right] \times e^{\left(\frac{\theta_c - \theta_c^{ref}}{\theta_0}\right)} \tag{9}$$

where T_{life} is the battery's service life, in years, decreases due to its degradation properties, N is the total number of half-cycles over the simulation period T, i is the index of the half-cycle, DOD_i is the DOD during the half-cycle i, θ_c is the case temperature, and θ_0 is the ambient temperature. $T_{calendar}^{ref}$ is the lifetime, in years, for a case temperature of θ_c^{ref}. In this study, a rainflow-counting algorithm is employed to determine all half-cycles. The parameters N_{cycles}^{ref}, $T_{calendar}^{ref}$, θ_0 and θ_c^{ref} are presented in Table 2 [31].

TABLE 2. Parameters of the Li-ion battery aging model.

N_{cycles}^{ref}	16,000
$T_{calendar}^{ref}$	25 years
θ_c^{ref}	25° C
θ_0	22 K

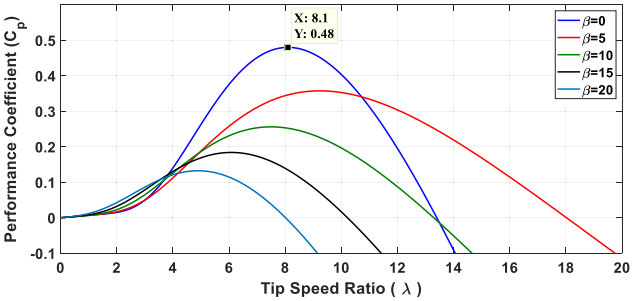

FIGURE 4. The C_p-λ characteristics of PMSG wind turbine.

TABLE 3. Parameters of the SC aging model.

θ_0	7.7 K
V_0	89 mV
K	29×10^{-3}
T_{life}^{ref}	1470 h
V^{ref}	2.7 V
θ_c^{ref}	65° C
K_{RMS}	68 s.V^{-1}

F. SC AGING MODEL

An aging model for the SC is adopted that considers both calendar aging and cycling aging [32]. The expected lifetime of the SC ($T_{SC,life}$) can be expressed as:

$$\frac{1}{T_{SC,life}} = \frac{1}{T_{life}^{ref}} \times \exp\left(\ln(2)\frac{\theta_c - \theta_c^{ref}}{\theta_0}\right) \times \left[\exp\left(\ln(2)\frac{V - V^{ref}}{V_0}\right) + K\right] \times \exp\left(K_{RMS}\frac{I_{RMS}}{C_0}\right) \tag{10}$$

where $T_{SC,life}$ is the SC lifetime in hours, θ_c is the case temperature and V is the voltage across the component. V_0 and θ_0 are the respective decreases in voltage and temperature necessary to double the SC service life. T_{life}^{ref} is the lifetime, in hours, for a case temperature of θ_c^{ref} with a voltage of V^{ref}. K is a dimensionless constant that replaces the voltage term whenever voltage is low. C_o is the initial value of the SC capacitance, and K_{RMS} is an accelerator factor. I_{RMS} is the RMS current flowing through the component. The parameters of the SC aging model are given in Table 3 [32].

G. DETERMINATION OF DISPATCH POWER REFERENCE

As mentioned earlier, the output of the PV array depends on two weather conditions: solar irradiation (W/m^2) and solar cell temperature (°C). Besides, the output of the WT depends on the wind's speed (m/s) through the rotor. In this study, the actual solar irradiance, temperature, and wind speed data recorded at NREL is utilized to predict the dispatched power on an hourly basis for an entire day, which is referred to as the $P_{Grid,ref}$. The $P_{Grid,ref}$ is estimated utilizing the average power that the WSHPS can provide over each dispatching period, and it serves as a target power level for the entire system. Thus, the WSHPS and HESS are committed to providing this target power to the utility grid for each hourly dispatching period for the entire duration. The four different data sets with diverse PV and WT output regimes, recorded at NREL on January 30th 2019, May 15th 2019, June 9th 2019 and September 30th, are collected to use in this study [13].

Here, the WSHPS framework consists of a 1 MW PV array and a 1.5 MW WT system. Thus, the average output power of the WSHPS over each dispatching period is a combination of the PV array's and WT system's output power. The average irradiation and temperature of the NREL solar data is utilized as inputs to the PV array to calculate the PV array's average output power over each dispatching period. The PV array module in Matlab/Simulink provides power-voltage characteristic curves based on user-input parameters, such as solar cell type, the number of cells in parallel, and the number of cells in series, under various weather conditions. The power-voltage characteristic curves for 1 MW PV array are shown in Fig. 5 and Fig. 6. At maximum power point (MPP) operation, the PV arrays' output power is marked as a circle of their respective curves. The resolution of the solar data recorded at NREL is one sample/minute. The cubic spline interpolation technique is employed to create a set of solar data with a resolution of 120 samples/minute and to map a value other than the four given maximum power points shown in Fig. 5 and Fig. 6. Afterwards, the average irradiation and temperature for each dispatching period are acquired utilizing the mean operation technique. The PVES estimated power from the average irradiation is referred as $P_{PVES,est}$ and the estimated efficiency of the PVES provided by the average temperature is referred to as $\eta_{PVES,est}$. Therefore, the final estimated power dispatchable by PVES (P_{PVES}) can be expressed as:

$$P_{PVES} = P_{PVES,est}(kW) \times \eta_{PVES,est}(\%) \tag{11}$$

Likewise, the estimated power dispatchable by WES (P_{WES}) is calculated in this study. The WT model in MATLAB/Simulink provides the WT power characteristic curve based on user input parameters such as base wind speed, base rotational speed, blade pitch angle (β), and maximum power at base wind speed. The WT power characteristics curve is illustrated in Fig. 7. In this power curve, β is assumed to be zero and wind speed varies from 5 m/s to 11 m/s.

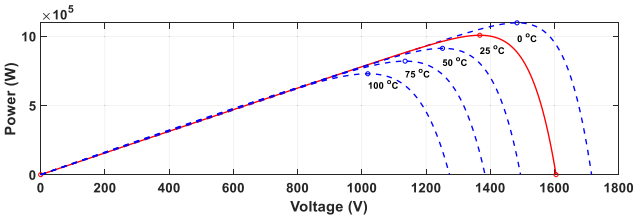

FIGURE 5. Power-Voltage characteristics of PV array at various temperatures.

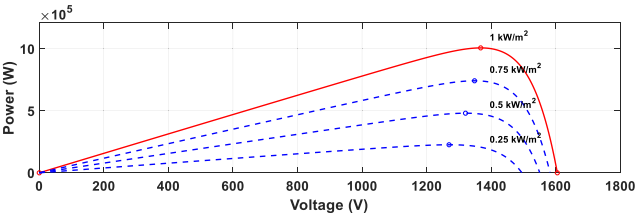

FIGURE 6. Power-Voltage characteristics of PV array at various irradiance.

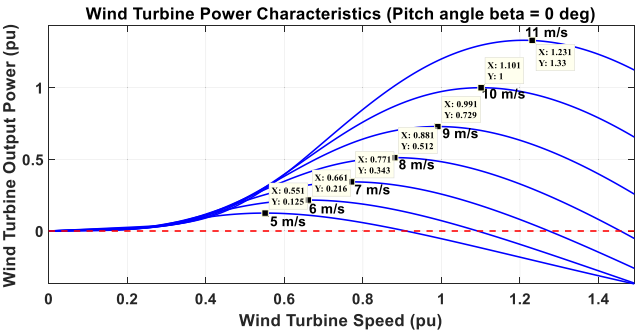

FIGURE 7. WT power characteristics curve.

The maximum power points for each wind speed are labelled. Then, cubic spline interpolation and mean operation techniques are implemented to acquire the average wind speed. The power level estimation from the average wind speed is referred to as the (P_{WES}). Finally, the average output power of the P_{WSHPS} is calculated by using (12). P_{WSHPS} is also referred to as the grid estimated power ($P_{Grid,est}$).

$$P_{Grid,est} = P_{PVES} + P_{WES} \tag{12}$$

Fig. 8 shows the block diagram deployed for the $P_{Grid,ref}$ calculation. It is critical to adjust the $P_{Grid,est}$ at the beginning of each period for achieving the desired $P_{Grid,ref}$ estimation, and minimizing the ESS cost. The multiplication factor for the $P_{Grid,est}$ correlates closely with the BESS SOC at the end of each dispatching period. This is accomplished by a rule-based algorithm that induces bounds represented by 10% SOC ranges that correspond to a multiplying factor. The ranges are from a battery SOC of 60% to 100% since one secondary SOC control algorithm is applied to guarantee the battery SOC regulates within this SOC limits. The resulting adjusted power level is referred as the $P_{Grid,ref}$. The primary SOC controller is employed to seek the desired multiplication factor for $P_{Grid,est}$ that ensures the ESS to

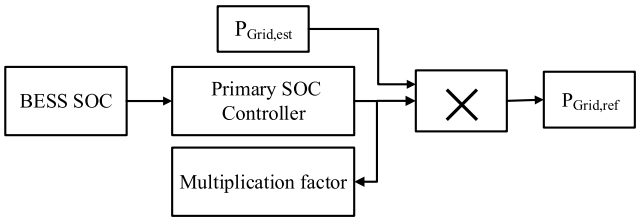

FIGURE 8. Block diagram of grid reference power calculation.

TABLE 4. $P_{Grid,ref}$ calculation from adjusting $P_{Grid,est}$ with BESS SOC.

BESS	Multiplication factor
100%≥SOC>92%	1.10
92%≥SOC>84%	1.05
84%≥SOC>76%	1.00
76%≥SOC>68%	0.95
68%≥SOC>60%	0.90

complete each dispatching period with the same SOC as it starts. Thus, the multiplication factor that is employed to adjust the $P_{Grid,est}$ plays a critical role in developing the most cost-effective ESS for hourly dispatching the WSHPS power.

To seek the appropriate multiplication factor to the $P_{Grid,est}$, a step rules algorithm, linearized step rules algorithm, and a fuzzy interference system are utilized as a primary SOC controller. Table 4 shows the rule-based control algorithm to calculate the $P_{Grid,ref}$ from adjusting the $P_{Grid,est}$ with BESS SOC [23]. The formula presented in (13) is employed to linearize the rule-based algorithm through regression analysis. Fig. 9 illustrates the linearization of the battery SOC. While implementing the fuzzy inference system, the BESS SOC is utilized as a fuzzy input, and the step rules algorithm shown in Table 4 is used in the rule editor. The output of the fuzzy inference system using the rules is shown in Fig. 10. Here, the fuzzy logic mechanism is utilized to implement a Mamdani type fuzzy inference system that exploits fuzzy logic for formulating the mapping from a given input to an output. Then the mapping provides a basis from which decisions can be made.

$$Multiplicationfactor = \frac{0.60 \times SOC + 51.7}{100} \tag{13}$$

H. CONTROL OF HESS

Fig. 11 shows the HESS control framework that is implemented in this research. Here, the HESS is responsible for regulating the system power, which is injected into the utility grid. The reference power for the HESS ($P_{HESS,ref}$) is the difference between the $P_{Grid,ref}$ and the P_{WSHPS}, which can be stated as:

$$P_{HESS,ref} = P_{Grid,ref} - P_{WSHPS} \tag{14}$$

The lifetime of the battery can degrade significantly when the fast changing (i.e., high-frequency) power components

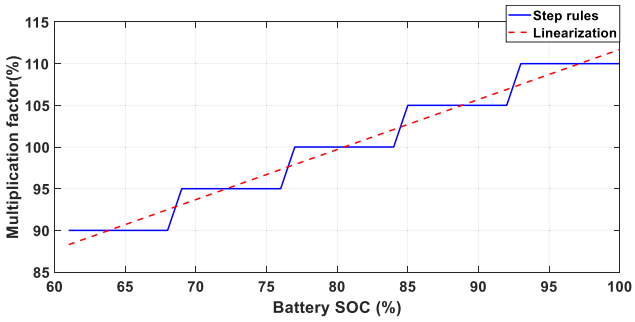

FIGURE 9. Linearization of step rules algorithm.

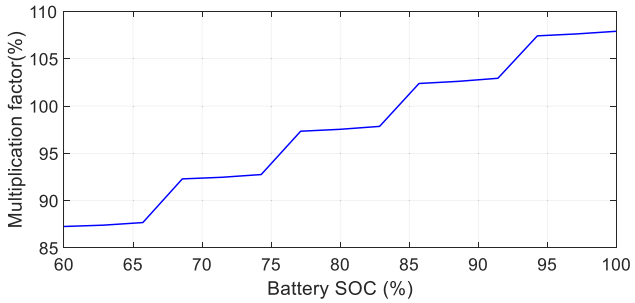

FIGURE 10. Output of the fuzzy inference.

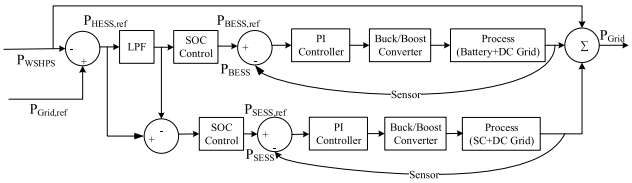

FIGURE 11. HESS power control framework.

flow through it. Thus, the $P_{HESS,ref}$ is sent through the LPF to allocate high-frequency components of power reference for the SESS ($P_{SESS,ref}$) and low-frequency components of power reference for the BESS ($P_{BESS,ref}$). In addition, after obtaining the optimal value of DOD ($DOD_{optimum}$) for the BESS, one rule-based SOC control algorithm is employed to regulate the BESS SOC in the optimal range. The block diagram of the rule-based algorithm for the BESS SOC control is illustrated in Fig 12. Likewise, another rule-based SOC control algorithm is implemented to regulate the SESS SOC after getting the optimal value of DOD for the SESS.

When the ESS is discharging (charging), the associated converter with the ESS acts in a boost (buck) mode in this HESS control architecture. The dc bus voltage demands to be set nearly twice as much as the ESS voltage for avoiding the discontinuity of the ESS input current induced by buck mode operation. The reference signals for the BESS and SESS are measured up to their instantaneous values (P_{BESS} for BESS, and P_{SESS} for SESS) to evaluate the duty ratio for the associated power converters. In this research, a pair of proportional integral (PI) controllers are applied for determining

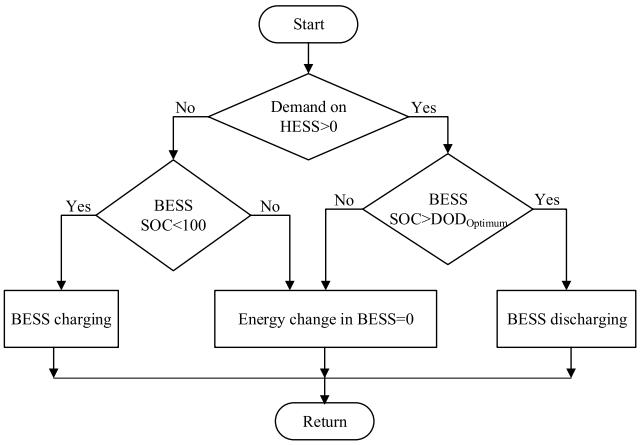

FIGURE 12. Rule-based algorithm for the BESS SOC control.

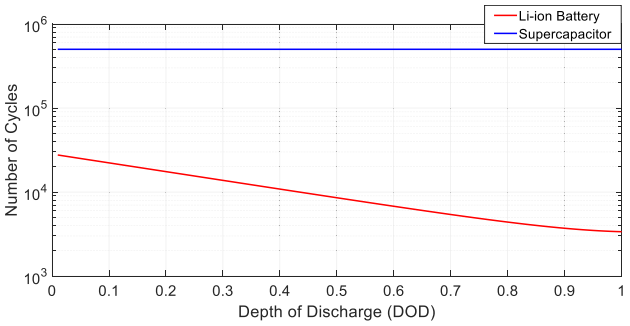

FIGURE 13. The relationship between DOD and cycle life.

the change in the duty ratio and reducing the proportional and integral error of the system.

I. HESS ENERGY AND POWER CAPACITY

To ensure the HESS can conform to the amount of energy that has to be charged or discharged, the minimum capacity demanded by the HESS needs to be determined. The energy capacity needed for the BESS and SESS is exploited through integrating the power profile of the BESS and SESS over each dispatching period respectively. At first, the absolute maximum amount of energy exploited by the BESS is computed through integrating the BESS power curve over each dispatching period and then in comparison to other dispatching period's maximum energy required for the BESS. Finally, (15) is utilized to determine the minimum capacity needed for the BESS to successfully dispatch the WSHPS power to the utility at one-hour increments for an entire day.

$$E_{BESS} = \frac{E_{sj}}{DOD_{max}} \tag{15}$$

where, E_{sj} is the total energy charged or discharged over the simulation period for the BESS, and DOD_{max} is the maximum DOD used by the BESS.

Likewise, the minimum capacity required for the SESS (E_{SESS}) is computed. Specifically, (16) is employed to calculate the required SC size.

$$E = \frac{1}{2}CV^2 \tag{16}$$

where E is the energy measured in Joules, C is the supercapacitor's capacitance measured in Farads, and V is the supercapacitor's voltage measured in Volt.

In this HESS power coordinated scheme, the positive P_{BESS} dictates that the BESS is discharging whereas the negative P_{BESS} dictates that the BESS is charging. Thus, the rated power capacity required for the BESS can be statistically quantified. At first, the absolute values of P_{BESS} over the simulation period are calculated. Then, its probability density function (PDF) and cumulative density function (CDF) are computed. Finally, the BESS rated power capacity ($P_{BESS,rated}$) is selected to be the values of $|P_{BESS}|$ which corresponds to the CDF of 1. Hence, the BESS can be expected to meet all the possible charging-discharging power requirements. Similarly, the rated power capacity for the SESS ($P_{SESS,rated}$) is evaluated in this study.

J. DOD OPTIMIZATION FOR HESS

The service life of the ESS primarily relies on the utilization of DOD and the rate of change of the charging-discharging power. The relationship between the cycle life and the DOD usage is close to exponential [33] and for the Li-ion battery it can be expressed as:

$$C_i = 28270e^{(-2.401DOD_i)} + 2.214e^{(5.901DOD_i)} \tag{17}$$

where C_i is the number of cycles when the depth of discharge is DOD_i. The relationship between DOD and cycle life calculated using (17) is shown in Fig. 13.

The expenditure associated with the ESS mainly depends on two factors, namely, (i) lifetime of the ESS and (ii) minimum capacity required for the ESS. Equation (15) illustrates that the minimum capacity required for the BESS is inversely proportional to the usage of its DOD. Nevertheless, deeper discharge of the BESS degrades its service life, as shown in Fig. 13. Thus, to determine the proper value of DOD that leads to the least expensive of the BESS ($/kWh) for dispatching the WSHPS power, the simulations are carried out considering every possible value of the BESS DOD. Likewise, the optimum value of the DOD for the SESS has been explored. Unlike the Li-ion battery, SC can be practically charged- discharged an infinite number of times. Hence, the total number of charging-discharging cycles for the SESS is considered to be constant (i.e., 500,000) in this investigation [34].

K. COST OPTIMIZATION FOR HESS

The LPF is employed to provide the power reference for the BESS and SESS. The minimum capacity needed for the SESS is directly proportional to the LPF time constant, while the minimum capacity needed for the BESS is inversely

proportional to the LPF time constant. A proper value of the filter time constant is required to minimize the total cost ($/kWh) of the HESS. Here, after acquiring the appropriate cost formula of the HESS as a function of the LPF time constant by utilizing the curve fitting method, the PSO approach is implemented to identify the optimum LPF time constant, as shown in Fig. 14. The mathematical formula of the HESS expenditure as a function of the LPF time constant is shown in (18), which is obtained employing the 4th order polynomial curve fitting method.

$$HESS_{Cost,LPF}(x) = P_1x^3 + P_2x^2 + P_3x + P_4 \quad (18)$$

where P_1, P_2, P_3 and P_4 are regression coefficients, and x is the LPF time constant, which is employed to distribute the power between the battery and SC in the HESS framework.

The PSO approach is incorporated due to its multiple advantages including: straightforward implementation, higher credibility in reaching the global optima, required for adaptation of few parameters, and speedy convergence. In general, the PSO offers a shorter evaluation time and better solution quality compared with a genetic algorithm, which is another optimization strategy usually deployed in renewable energy systems. The PSO performs a search for the feasible solutions, called particles, flying through the problem space by following the current optimum particles. The model of the particle's position can be expressed as:

$$V_i^{k+1} = wV_i^k + C_1 rand_1 \times (pbest_i - S_i^k) + C_2 rand_2 \times (gbest - S_i^k) \quad (19)$$

$$S_i^{k+1} = S_i^k + V_i^{k+1} \quad (20)$$

where ${V_i}^{k+1}$ is the velocity of agent i at the iteration k, w is the weighting function, C_j is the weighting factor, *rand* is the uniformly distributed random number between 0 and 1, ${S_i}^k$ the current position of agent i at the iteration k, p_{best_i} is the personal best position of agent i, and *gbest* is the global best position of the group.

L. EXPECTED LIFETIMES OF THE BESS AND SESS

Due to the intermittent nature of the WSHPS output power, the charging-discharging characteristics of the BESS over a period is used to estimate the service life of the BESS. Here, the equation to compute the equivalent service cycle life ($C_{B,T}$) of the BESS over the period T_s is shown below:

$$C_{B,T} = \sum_{j \in T_s} \frac{E_{sj}}{E_{BESS}} \quad (21)$$

where, E_{sj} is the total energy charged or discharged (whichever is greater) over the simulation period T_s. E_{BESS} is battery's rated energy capacity multiplied by DOD and a correction factor to derate manufacturer's data (a correction factor of 0.8 is assumed in this study). Accordingly, the expected lifetime of the battery $E|L_B|$ is calculated using (22):

$$E|L_B| = \frac{C_{B,n}}{C_{B,T}} \times T_s \quad (22)$$

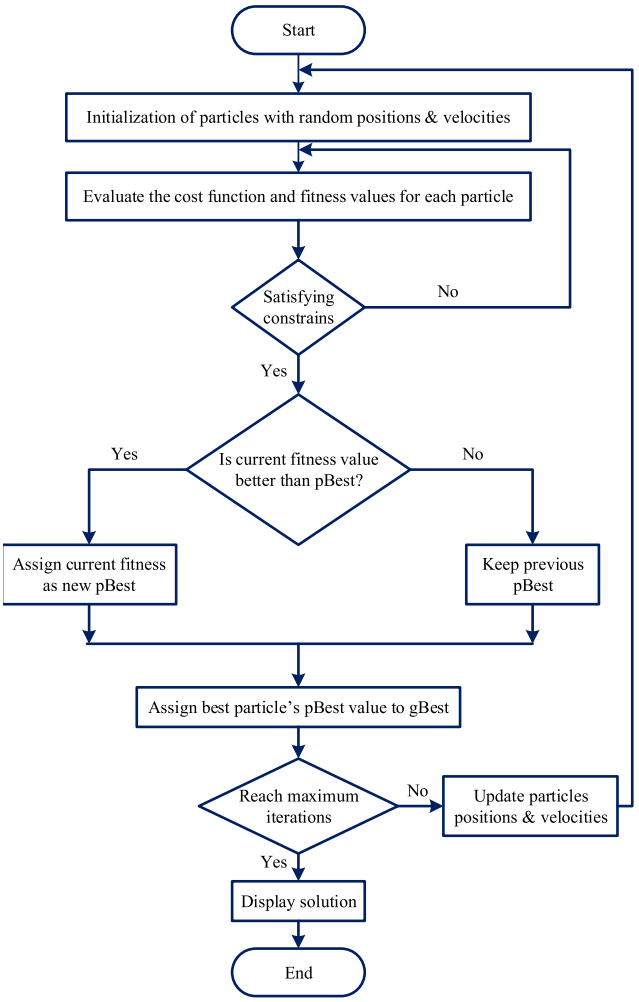

FIGURE 14. PSO functional flowchart.

where $C_{B,n}$ is the life cycle of the battery provided by the manufacturers.

The expected lifetime of the BESS deteriorates due to its calendar aging and this is also contemplated here. The BESS degradation model has been explained in Section III.E. T_{life} in (9) reflects the decline of the BESS service life due to its calendar aging. The SESS aging model that considers both cycling and calendar aging is adopted in this study. The SESS aging model has been fully documented in Section III.F. Hence, $T_{SC,life}$ in (10) indicates the expected lifetime of the SESS, while accounting for both cycling and calendar aging.

M. COST CALCULATION FOR HESS

Both cycling and calendar aging expenses are considered while the ESS cost is investigated in this research. The overall expenditure of the ESS includes its capital cost, power conversion system cost, and operation and maintenance (O&M) cost. Therefore, the total expense associated with the BESS ($C_{Bat,Total}$) can be estimated by using (23):

$$C_{Bat,Total}(\$) = C_{Cap} + C_{Conv} + C_{O\&M} \quad (23)$$

where C_{Cap} is the BESS capital cost, C_{Conv} is the BESS power conversion system cost, and $C_{O\&M}$ is the BESS operation and maintenance cost.

The capital cost of the BESS (C_{Cap}) can be expressed by:

$$C_{Cap} = C_{cycling} + C_{calendar} \tag{24}$$

$$C_{Cap} = \frac{E_{BESS} \times C_B}{E|L_B|} + \frac{E_{BESS} \times C_B}{T_{life}} \tag{25}$$

where $C_{cycling}$ and $C_{calendar}$ are the cycling and calendar expenses associated with the BESS respectively. E_{BESS} is the required energy capacity of the BESS in kWh, C_B is the BESS capital cost ($/kWh), $E|L_B|$ is the expected lifetime of the BESS and T_{life} is the expected lifetime of the BESS deteriorates due to its calendar aging.

The power conversion system expense of the BESS (C_{Conv}) can be expressed by:

$$C_{Conv} = \frac{P_{BESS,rated} \times P_B}{E|L_B|} + \frac{P_{BESS,rated} \times P_B}{T_{life}} \tag{26}$$

where $P_{BESS,rated}$ is the required power capacity of the BESS in kW and P_B is the BESS power conversion system cost ($/kW). Likewise, the BESS O&M expenditure is evaluated in this research.

In this study, $T_{SC,life}$ indicates the expected lifetime of the SESS that considers both cycling and calendar aging. Thus, the capital cost of the SESS (SC_{Cap}) can be expressed by:

$$SC_{Cap} = \frac{E_{SESS} \times C_{SC}}{T_{SC,life}} \tag{27}$$

where E_{SESS} is the required energy capacity of the SESS in kWh and C_{SC} is the SESS capital cost ($/kWh).

The power conversion system expenditure of the SESS (SC_{Conv}) can be expressed by:

$$SC_{Conv} = \frac{P_{SESS,rated} \times P_{SC}}{T_{SC,life}} \tag{28}$$

where $P_{SESS,rated}$ is the required power capacity of the SESS in kW and P_{SC} is the SESS power conversion system cost ($/kW). Likewise, the SESS O&M expense ($SC_{O\&M}$) is computed in this study.

Therefore, the total cost associated with the SESS ($C_{SC,Total}$) can be calculated by using (29):

$$C_{SC,Total}(\$) = SC_{Cap} + SC_{Conv} + SC_{O\&M} \tag{29}$$

Finally, the normalized HESS cost per kWh can be expressed as follows:

$$C_{HESS}(\$) = C_{Bat,Total} + C_{SC,Total} \tag{30}$$

$$Cost_{Norm} = \frac{C_{HESS}}{(P_{PV} \times PV_{CF} + P_{WT} \times WT_{CF}) \times T} \tag{31}$$

where P_{PV} is the PV array capacity (kW), PV_{CF} is the PV capacity factor (20% is assumed in this study), P_{WT} is the wind turbine capacity (kW), WT_{CF} is the wind turbine capacity factor (35% is assumed in this study), and T is the number of hours in a year. The unit price and life cycle of different energy storage exploited in this study are summarized in Table 5 [35].

TABLE 5. Battery and SC cost comparison.

Parameter	Battery	SC
Capital cost	271 ($/kWh)	2500 ($/kWh)
Power conversion system	271 ($/kW)	350 ($/kW)
O&M-Fixed	10 ($kW-year)	1 ($/kW-year)
O&M-Variable	3 ($kWh)	3 ($/kWh)
Charging-discharging cycles	10,000 (40%DOD)	500,000

IV. SIMULATION RESULTS

In this research, the hourly dispatching WSHPS has been developed and simulated in MATLAB/Simulink^{TM} environment. Furthermore, bidirectional power converters, three-level T-type inverter, LCL filter, and the corresponding control algorithms have been modelled and analyzed to justify the performance and the economic evaluation of the HESS architecture.

Fig. 15 illustrates the power profiles of the WSHPS, HESS, P_{Grid}, and $P_{Grid,ref}$. Here, the P_{Grid} is the combination of the WSHPS and HESS power injected into the grid by an inverter, and the $P_{Grid,ref}$ is utilized as a target power level for the WSHPS and HESS to supply to the grid. It is noticeable that the P_{Grid} remains constant in each dispatching period and successfully follows the desired $P_{Grid,ref}$. Hence, it can be concluded that the HESS successfully contributes the necessary power either by supplying or absorbing to provide a constant power to the utility from the intermittent WSHPS architecture. Further investigation into the simulation results also validates the fact that the fast-changing components of the power are charged-discharged by the SESS while the slow-changing components of the power are charged-discharged by the BESS.

The $P_{Grid,ref}$ for the WSHPS is generated utilizing two different schemes, i.e., (i) dispatchable power reference case—estimating the $P_{Grid,ref}$ utilizing the approach elucidated in Section III.G. and (ii) load following case—load profile for 2.5 MW utility is collected from CAISO and is utilized as a grid reference power for the entire system. Fig. 15 illustrates the simulation result for the dispatchable power reference case and Fig. 16 demonstrates the simulation result for the load following case. It is worth mentioning that the P_{Grid} successfully follows the desired $P_{Grid,ref}$ in both cases investigated in this study.

In addition, to validate the effectiveness of the proposed HESS control framework, a one-hour simulation has been carried out considering all possible cases of the availability of sources investigated in this study—(i) PV+WT+ESS (ii) WT+ESS (iii) PV+ESS (iv) ESS only—to dispatch the desired grid reference power for the entire duration. Fig. 17 illustrates the one-hour simulation results, and it is shown that the proposed control framework is capable of dispatching the desired $P_{Grid,ref}$ irrespective of the availability of renew-

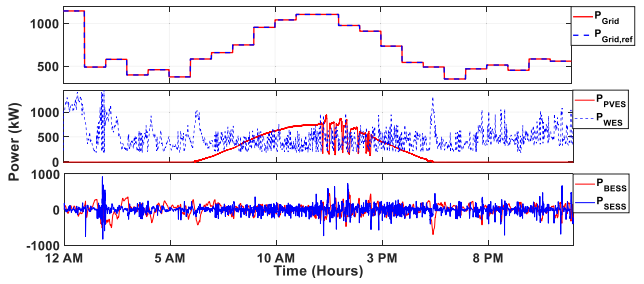

FIGURE 15. Dispatchable power reference case: Simulation results for one-hour dispatching for September 30th, 2019.

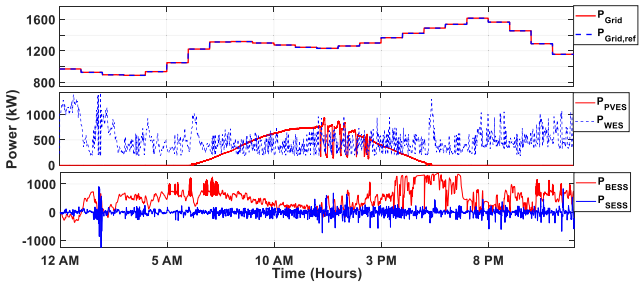

FIGURE 16. Load following case: Simulation results for one-hour dispatching for September 30th, 2019.

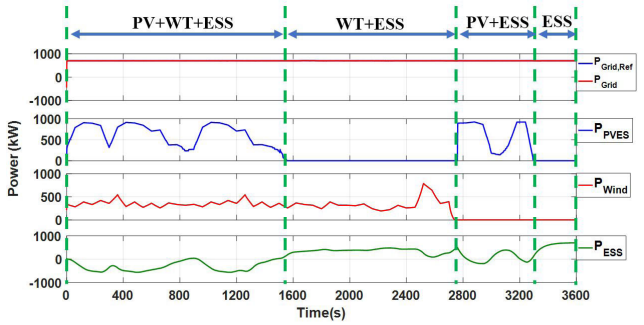

FIGURE 17. One-hour simulation results considering all possible cases of the availability of sources.

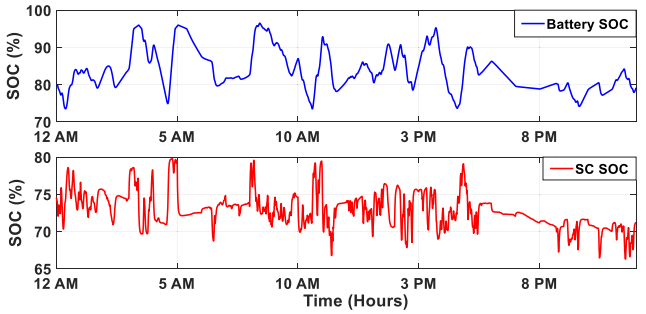

FIGURE 18. Simulation results of the SOC with the battery and SC.

able energy sources. Note that even though the proposed architecture can effectively operate in the ESS-only mode to fulfill the desired $P_{Grid,ref}$ in each dispatching period, the required ESS capacity will become unnecessarily large in this scenario. Therefore, the ESS-only mode might not be cost-effective for hourly dispatching the WSHPS power to the grid.

The primary SOC controller as a function of the BESS SOC is developed to ensure the BESS finishes each dispatching period with the same SOC as it started. This type of SOC constraint is demanded for estimating the desired $P_{Grid,ref}$, minimizing the BESS cost, and ensuring the BESS has enough capacity to be available for the next-day operation. The simulation result of the BESS SOC variation on September 30th 2019 is illustrated in Fig. 18, which highlights the effectiveness of the primary SOC controller to regulate the BESS SOC within a specified range. As mentioned before, a step rules algorithm, linearized step rules algorithm, and a fuzzy interference system are employed as a primary SOC controller to seek the appropriate multiplication factor to the $P_{Grid,est}$ in this study. The effect of those algorithms on the HESS cost assessment is demonstrated in Fig. 19 for September 30th 2019 meteorological data. The performances of the algorithms do not differ substantially, and fuzzy logic rule approach performs slightly better.

In this paper, the simulations are carried out considering every possible value of the BESS DOD to seek the optimum value of DOD that exhibits the least cost ($/kWh) of the BESS for hourly dispatching the WSHPS power. The BESS cost per kWh as a function of its usage of DOD is illustrated in Fig. 20. As shown in Fig. 20, the optimum value of the BESS DOD that demonstrates the minimum cost is found at 42% DOD, which is approximately 9.85 ¢/kWh in the case of September 30th 2019 simulation.

The SESS cost per kWh as a function of its usage of DOD is also demonstrated in Fig. 20. It is observed that the full utilization of the SESS results in the least cost. The expenditure associated with the ESS is inversely proportional to the service life of the ESS and is directly proportional to the ESS capacity. Since the SC can be charged-discharged a virtually unlimited number of times, the total number of charging-discharging cycles of the SC as a function of its DOD usage, in any event, remained constant, as demonstrated in Fig. 13. Furthermore, the capacity needed for the SC becomes minimum when it is fully exploited. Consequently, at 100% DOD, the SESS demonstrates the least cost, approximately 17.2 ¢/kWh in the case of September 30th 2019 simulation. For better illustration, the ESS expense as a function of its DOD usage in the range between 10% to 100% is illustrated in Fig. 20.

In order to investigate the impact of utilizing different types of ESS for hourly dispatching the WSHPS power, an economic comparison is presented in Table 6. From Table 6, it is noted that the HESS can be the most cost-effective framework compared with the battery or SC-only operation. In addition, the following three steps are taken into account to seek the optimum LPF time constant. (1) A real meteorological dataset (i.e., September 30th 2019) with the solar irradiance, temperature, and wind speed profile that has considerable fluctuations is integrated into the Simulink model to carry

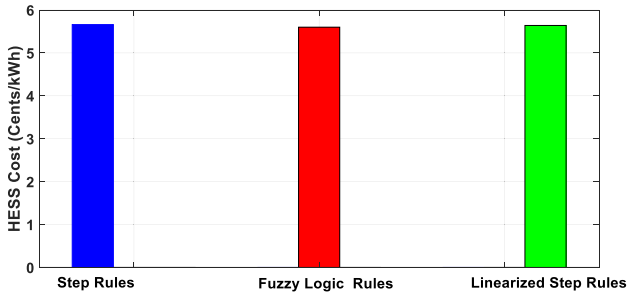

FIGURE 19. HESS cost comparison at different primary SOC control algorithms.

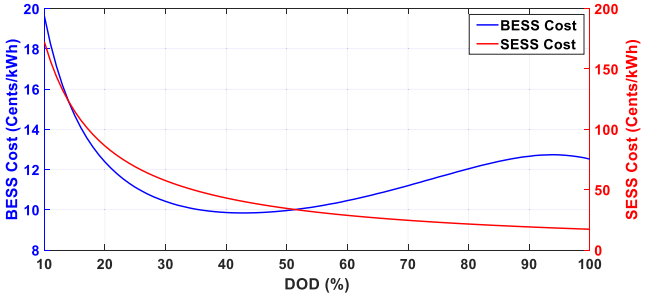

FIGURE 20. ESS cost (¢/kWh) at different DOD levels.

TABLE 6. Energy storage cost comparison at different LPF time constants.

LPF time constant (s)	0	60	120	180	240	∞
Cost (¢/kWh)	9.85	5.62	7.33	9.27	10.16	17.20

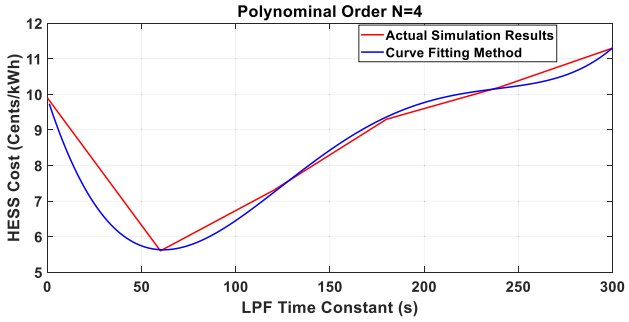

FIGURE 21. Simulation results using the optimization method.

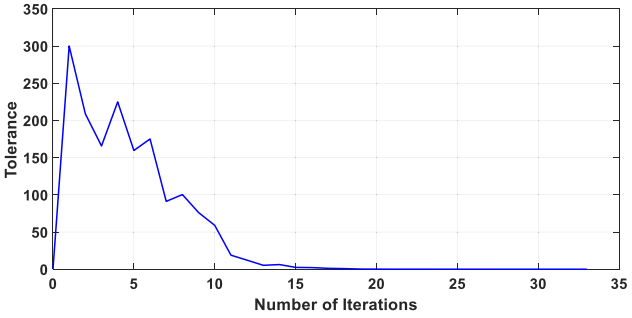

FIGURE 22. Convergence rate of the PSO technique.

out the simulations at different LPF time constants, as is presented in 6. (2) The curve fitting approach is executed to develop the best mathematical cost equation of the HESS as a function of the LPF time constants, as illustrated in Fig. 21. (3) Finally, the PSO strategy is applied by utilizing the HESS cost equation to seek the most feasible LPF time constant. In this study, the most optimum HESS cost is found at 62s LPF time constant by using the 4th order polynomial HESS cost equation. The convergence rate of the PSO technique is illustrated in Fig. 22.

There are two main constraints took into account in the course of the cost optimization process, namely, (i) total power supplied from the WSHPS farm (P_{Grid}) must cover the desired $P_{Grid,ref}$ in each dispatching period, and (ii) SOC of the BESS and SESS remains above the specified DOD. Fig. 15, Fig. 16 and Fig. 18 are presented to validate these optimization constraints.

To obtain the annual energy storage cost for hourly dispatching the WSHPS power, the four different datasets as representative of four seasons recorded by U.S. NREL, are utilized in this study [13]. The annual HESS expenditure is estimated by the weighted average value of the four different seasons' energy storage costs. The HESS cost comparison at the optimum LPF time constant (i.e., 62s) between the dispatchable power reference case and the load following case is illustrated in Fig. 23. In the dispatchable power reference case, the $P_{Grid,ref}$ is determined by estimating the average power that the WSHPS can provide over each dispatching period. In the load following case, the load profile for 2.5 MW utility is collected from CAISO and is utilized as the $P_{Grid,ref}$ for the entire system. The P_{Grid} successfully follows the desired $P_{Grid,ref}$ in both cases investigated in this study, as shown in Fig. 15 and Fig. 16.

Due to the capacity factor constraints of renewable energy sources, when the WSHPS framework is assigned to meet the load demand that is equal to the WSHPS rated capacity, the WSHPS framework demands significant contribution from the ESS to successfully meet the utility load profile. Consequently, the required ESS capacity increases substantially for the load following case, as illustrated in Fig. 16. Thus, the HESS cost (¢/kWh) is found to be more expensive for the load following case than the dispatchable power reference case. It is expected that the transmission system operator (TSO) assigns the load demand for the WSHPS framework considering the capacity factor constraints of renewable energy sources. Since the WSHPS is utilized to fulfill its rated load demand without considering the capacity factor constraints, the HESS cost (¢/kWh) reflects the worst-case scenario for the load following case.

The HESS expense is directly proportional to the required ESS size but is inversely proportional to the PV or WT capacity factor. The collaborative capacity factor of the WSHPS is higher than the individual PV or WT system. Also, the required ESS size is reduced in the WSHPS to fulfill the grid power demand due to the complementary power profiles

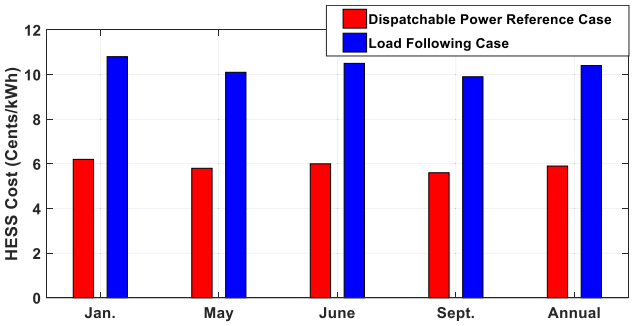

FIGURE 23. HESS cost (¢/kWh) at 62s of the LPF time constants.

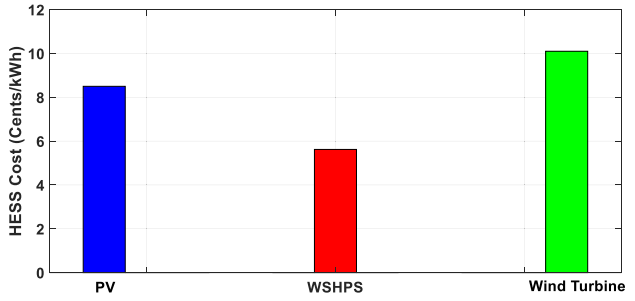

FIGURE 24. Annual HESS cost comparison at 62s of the LPF time constants.

of the WT and PV. Thus, the cost of the HESS becomes minimum in the WSHPS in comparison with a single PV or WT framework, which is verified in Fig. 24.

In this study, the statistical approach is performed to illustrate the required ESS capacities at different cumulative probability density function levels. The cumulative probability density function of the BESS energy capacities and the SESS energy capacities at 62s LPF time constant for the dispatchable power reference case are demonstrated in Fig. 25, which shows that there is a trade-off between the loss of power supply probability and the minimum capacity required of the ESS. Since the ESS is committed to meet all of the possible charging-discharging energy requirements in this hourly dispatching scheme, the ESS rated energy capacity is chosen corresponding to the CDF of 1, which is one factor to increase the required ESS capacity. Here, the most economical size of the BESS and SESS combination in the HESS scheme turns out to be 354 kWh and 55 kWh respectively at 62s LPF time constant for the dispatchable power reference case. Likewise, the required power capacities of the BESS and SESS are evaluated for the HESS economic assessment.

The percentage of error between the P_{Grid} and $P_{Grid,ref}$ is computed using (32) to quantify the power quality criteria. The histogram of this error percentage is demonstrated in Fig 26. Since the P_{Grid} successfully tracks the desired $P_{Grid,ref}$ closely in each dispatching period, the undesired deviation is found to be extremely low for the dispatchable power reference case. The similar phenomenon of the undesired deviation is also observed for the load following case. This attribute indicates the effectiveness of dispatchability

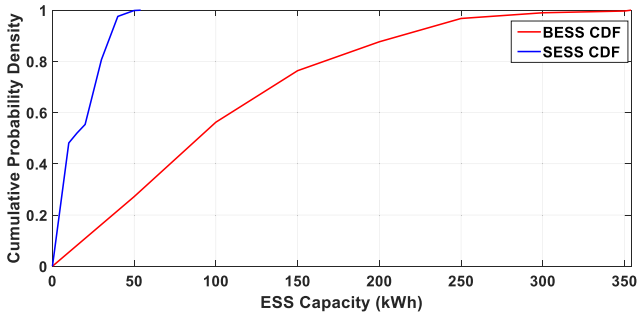

FIGURE 25. Cumulative probability density function of the BESS energy capacities.

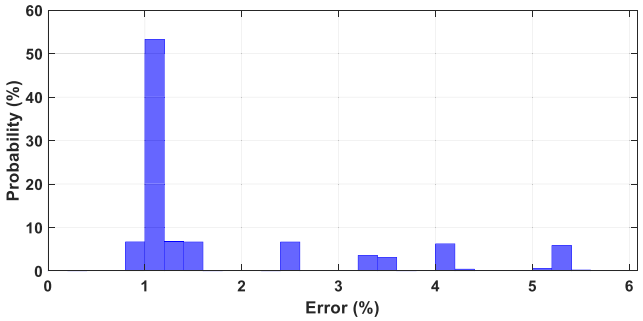

FIGURE 26. Histogram of hourly dispatching error results.

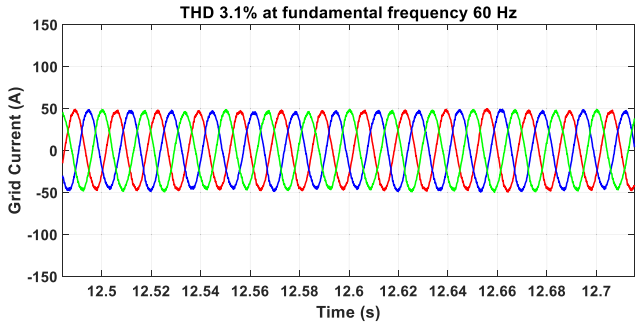

FIGURE 27. Injected current into the grid.

provided by the WSHPS and HESS framework.

$$Error(\%) = \frac{|P_{Grid,ref} - P_{Grid}|}{P_{Grid,ref}} \tag{32}$$

Furthermore, IEEE 1547–2003 [36] provides the THD constraints of the grid voltage and current for the interconnection of distributed resources within electric power systems to maintain the power quality of the utility grid. The three-phase current injected into the grid is illustrated in Fig. 27, and the THD of the injected current is found to be 3.1%, which is within reasonable limits. Furthermore, the three-phase grid voltage waveform is shown in Fig. 28, and the THD of the grid voltage waveform is found to be 0.12%, which is within reasonable limits as well.

As mentioned earlier, the expenditure associated with the ESS is inversely proportional to its lifetime. The SESS helps to alleviate the fast-changing power components passing

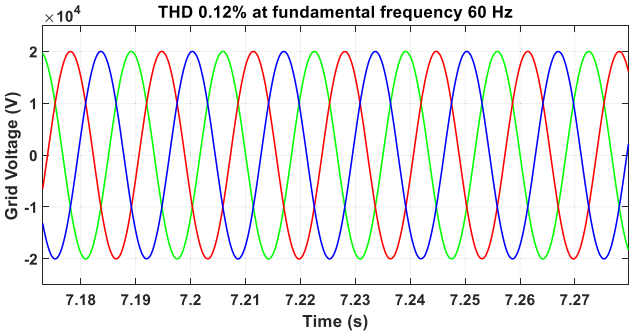

FIGURE 28. Three-phase voltage waveforms of the grid.

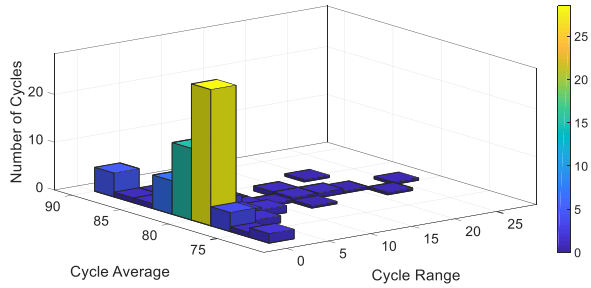

FIGURE 29. Rainflow matrix histogram of the BESS.

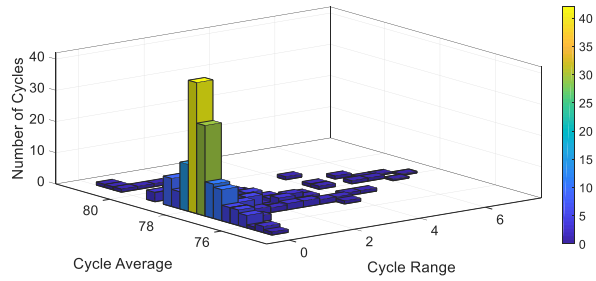

FIGURE 30. Rainflow matrix histogram of the SESS.

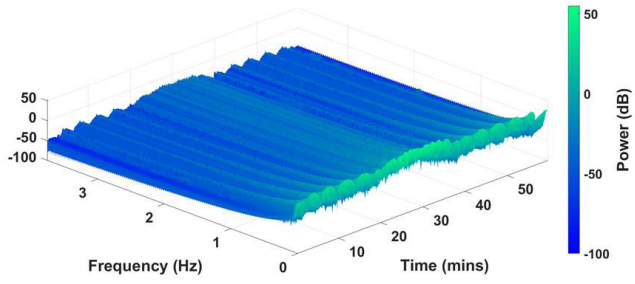

FIGURE 31. Spectrogram of the BESS.

through the BESS in the HESS architecture, which is beneficial for prolonging the BESS service life. In the rainflow counting approach, cycle range signifies the absolute value of the difference between the amplitude of the first point and the second point when the cycle is considered. Fig. 29 illustrates the rainflow histogram of the BESS to validate the fact that the slow-changing components of the HESS power are charged-discharged through the BESS.

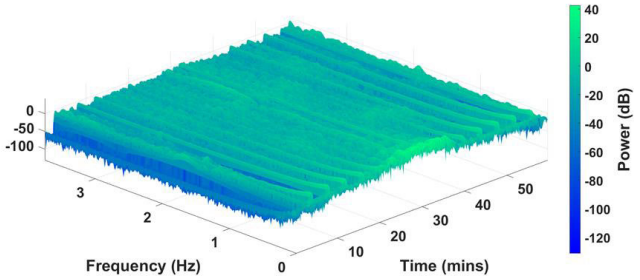

FIGURE 32. Spectrogram of the SESS.

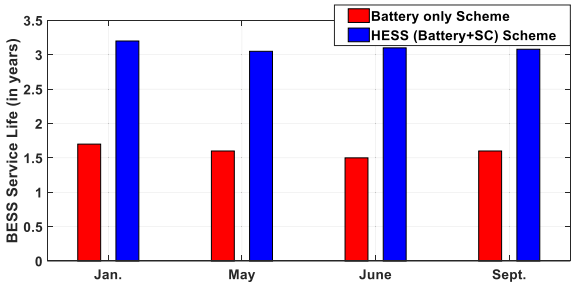

FIGURE 33. Battery lifetime (in years) comparison.

Nevertheless, the fast-changing components of the HESS power are charged-discharged through the SESS. Fig. 30 is presented to justify this statement.

Furthermore, the power spectral density of the BESS and SESS shown in Fig. 31 and Fig. 32 exhibits the relative effectiveness of the SESS for absorbing high frequency components from the HESS. An estimated BESS lifetime comparison with and without the SESS in the energy storage framework is illustrated in Fig. 33. It can be observed that the BESS lifetime substantially increases when the SESS is part of the storage framework. Hence, the HESS is more cost-effective in comparison to using battery-only for dispatching the WSHPS power to the utility grid.

V. CONCLUSION

In this study, an hourly dispatching scheme of the WSHPS power has been presented. Simulation results exhibit that the WSHPS power can be successfully dispatched on an hourly basis at an error of less than approximately 1.5% most of the time. Thus, by deploying the ESS control method investigated in this research, the WSHPS can be utilized as a reliable source of power to afford the base load demand.

The cost optimization of the ESS is one of the important catalysts for the significant development of renewable energy generation. In this paper, the energy storage life cycle cost is optimized as a function of its DOD usage. Furthermore, the optimum value of the LPF time constant in the HESS architecture has been found to be 62s by implementing the curve fitting and PSO techniques that yield the most cost-effective HESS (i.e., annual HESS cost 5.9 ¢/kWh and 10.3 ¢/kWh for the grid dispatchable power case and the load following case, respectively). The significance of the SC on battery longevity when it is integrated into the HESS

framework has been investigated. Also, the impact of the SOC control algorithms has been validated to develop a cost-effective HESS for a utility-scale hybrid PV-WT system.

Since the computer simulation for one-day solar-wind data requires a significant amount of time to complete, the annual energy storage is computed utilizing the four diverse days of solar-wind data in this investigation. In the future, a more comprehensive study about annual energy storage expenditure will be explored by selecting more days for solar-wind data and employing higher processing power for simulations. Besides, the impact of the SC SOC in the grid reference estimation algorithm will be investigated to make the system more practical. Implementing the multi-port power converter for interfacing the PV and HESS is another topic for our future work.

REFERENCES

[1] Energy Information Administration (EIA). (2020). *Renewable Energy Explained*. Accessed: Jun. 27, 2020. [Online]. Available: https://www.eia.gov/energyexplained/renewable-sources/
[2] *Renewables 2019 Global Status Report*. Accessed: May 20,2020. [Online]. Available: https://www.ren21.net/wp-content/uploads
[3] California ISO, NREL, and First Solar. *Using Renewables to Operate a Low-Carbon Grid: Demonstration of Advanced Reliability Services From a Utility-Scale Solar PV Plant*. Accessed: May 17, 2020. [Online]. Available: https://www.caiso.com
[4] A. Andreas and T. Stoffel, "NREL solar radiation research laboratory (SRRL): Baseline measurement system (BMS)," NREL, Golden, CO, USA, Tech. Rep. DA-5500-56488, 1981.
[5] J. L. Bernal-Agustín and R. Dufo-López, "Simulation and optimization of stand-alone hybrid renewable energy systems," *Renew. Sustain. Energy Rev.*, vol. 13, no. 8, pp. 2111–2118, Oct. 2009.
[6] Tilitydive. *NextEra inks 700 Mw Wind + Solar + Battery Project, Largest in the US*. Accessed: Aug. 10, 2020. [Online]. Available: https://www.utilitydive.com/news/nextera-inks-700-mw-wind-solar-battery-project-largest-in-the-us/559693/
[7] R. Carnegie, D. Gotham, D. Nderitu, and P. V. Preckel, "Utility scale energy storage systems: Benefits, applications, and technologies," State Utility Forecasting Group (SUFG), Purdue Univ., West Lafayette, IN, USA, Tech. Rep., 2013.
[8] J. Kondoh, "Stationary applications. Load levelling," in *Industrial Applications of Batteries*, M. Brousselyon and G. Pistoia, Eds. Amsterdam, The Netherlands: Elsevier, 2007, p. 462, 465, 470–477.
[9] S. K. Kollimalla, M. K. Mishra, and N. L. Narasamma, "Design and analysis of novel control strategy for battery and supercapacitor storage system," *IEEE Trans. Sustain. Energy*, vol. 5, no. 4, pp. 1137–1144, Oct. 2014.
[10] H. Chen, T. N. Cong, W. Yang, C. Tan, Y. Li, and Y. Ding, "Progress in electrical energy storage system: A critical review," *Prog. Natural Sci.*, vol. 19, no. 3, pp. 291–312, Mar. 2009.
[11] M. E. Glavin, P. K. W. Chan, S. Armstrong, and W. G. Hurley, "A stand-alone photovoltaic supercapacitor battery hybrid energy storage system," in *Proc. 13th Int. Power Electron. Motion Control Conf.*, Poznan, Poland, Sep. 2008, pp. 1688–1695.
[12] L. Bird, M. Milligan, and D. Lew, "Integrating variable renewable energy: Challenges and solutions," Nat. Renew. Energy Lab. (NREL), Golden, CO, USA, Tech. Rep. NREL/TP-6A20-60451, 2013, doi: 10.2172/1097911.
[13] D. Jager and A. Andreas, "NREL national wind technology center (NWTC): M2 Tower," Nat. Renew. Energy Lab., Boulder, CO, USA, NREL Rep. DA-5500-56489, 2014.
[14] S. Teleke, M. E. Baran, S. Bhattacharya, and A. Q. Huang, "Rule-based control of battery energy storage for dispatching intermittent renewable sources," *IEEE Trans. Sustain. Energy*, vol. 1, no. 3, pp. 117–124, Oct. 2010.
[15] S. Teleke, M. E. Baran, A. Q. Huang, S. Bhattacharya, and L. Anderson, "Control strategies for battery energy storage for wind farm dispatching," *IEEE Trans. Energy Convers.*, vol. 24, no. 3, pp. 725–732, Sep. 2009.
[16] M. Z. Daud, A. Mohamed, and M. A. Hannan, "An improved control method of battery energy storage system for hourly dispatch of photovoltaic power sources," *Energy Convers. Manage.*, vol. 73, pp. 256–270, Sep. 2013.
[17] X. Y. Wang, D. M. Vilathgamuwa, and S. S. Choi, "Determination of battery storage capacity in energy buffer for wind farm," *IEEE Trans. Energy Convers.*, vol. 23, no. 3, pp. 868–878, Sep. 2008.
[18] Q. Li, S. S. Choi, Y. Yuan, and D. L. Yao, "On the determination of battery energy storage capacity and short-term power dispatch of a wind farm," *IEEE Trans. Sustain. Energy*, vol. 2, no. 2, pp. 148–158, Apr. 2011.
[19] C.-L. Nguyen, H.-H. Lee, and T.-W. Chun, "Cost-optimized battery capacity and short-term power dispatch control for wind farm," *IEEE Trans. Ind. Appl.*, vol. 51, no. 1, pp. 595–606, Jan. 2015.
[20] D. L. Yao, S. S. Choi, K. J. Tseng, and T. T. Lie, "Determination of short-term power dispatch schedule for a wind farm incorporated with dual-battery energy storage scheme," *IEEE Trans. Sustain. Energy*, vol. 3, no. 1, pp. 74–84, Jan. 2012.
[21] D. L. Yao, S. S. Choi, K. J. Tseng, and T. T. Lie, "A statistical approach to the design of a dispatchable wind power-battery energy storage system," *IEEE Trans. Energy Convers.*, vol. 24, no. 4, pp. 916–925, Dec. 2009.
[22] K. W. Wee, S. S. Choi, and D. M. Vilathgamuwa, "Design of a least-cost battery-supercapacitor energy storage system for realizing dispatchable wind power," *IEEE Trans. Sustain. Energy*, vol. 4, no. 3, pp. 786–796, Jul. 2013.
[23] J. Chaires, H. B. Karayaka, Y. Yan, and P. Gardner, "Solar farm hourly dispatching using super-capacitor and battery system," in *Proc. Clemson Univ. Power Syst. Conf. (PSC)*, Clemson, SC, USA, Mar. 2016, pp. 1–7.
[24] P. K. S. Roy, H. B. Karayaka, Y. Yan, and Y. Alqudah, "Size optimization of battery-supercapacitor hybrid energy storage system for 1MW grid connected PV array," in *Proc. North Amer. Power Symp. (NAPS)*, Morgantown, WV, USA, Sep. 2017, pp. 1–6.
[25] P. K. S. Roy, H. B. Karayaka, Y. Yan, and Y. Alqudah, "Evaluation of reference generation algorithms for dispatching solar PV power," in *Proc. SoutheastCon*, St. Petersburg, FL, USA, Apr. 2018, pp. 1–7.
[26] P. K. S. Roy, H. B. Karayaka, Y. Yan, and Y. Alqudah, "Investigations into best cost battery-supercapacitor hybrid energy storage system for a utility scale PV array," *J. Energy Storage*, vol. 22, pp. 50–59, Apr. 2019.
[27] H. Zheng, S. Li, C. Zang, and W. Zheng, "Coordinated control for grid integration of PV array, battery storage, and supercapacitor," in *Proc. IEEE Power Energy Soc. Gen. Meeting*, Vancouver, BC, Canada, Jul. 2013, pp. 1–5.
[28] A. M. Atallah, A. Y. Abdelaziz, and R. S. Jumaah, "Implementation of perturb and observe MPPT of PV system with direct control method using buck and buck-boost converters," *Emerg. Trends Elect., Electron. Instrum. Eng., Int. J.*, vol. 1, no. 1, pp. 31–44, Feb. 2014.
[29] L. Djamel and B. Abdallah, "Power quality control strategy for grid-connected renewable energy sources using PV array, wind turbine and battery," in *Proc. 4th Int. Conf. Power Eng., Energy Electr. Drives*, Istanbul, Turkey, May 2013, pp. 1671–1675.
[30] M. Muzathik, "Photovoltaic modules operating temperature estimation using a simple correlation," *Int. J. Energy Eng.*, vol. 4, no. 4, pp. 151–158, 2014.
[31] T. Kovaltchouk, H. Ben Ahmed, B. Multon, J. Aubry, and P. Venet, "An aging-aware life cycle cost comparison between supercapacitors and Li-ion batteries to smooth direct wave energy converter production," in *Proc. IEEE Eindhoven PowerTech*, Eindhoven, The Netherlands, Jun. 2015, pp. 1–6.
[32] T. Kovaltchouk, B. Multon, H. Ben Ahmed, J. Aubry, and P. Venet, "Enhanced aging model for supercapacitors taking into account power cycling: Application to the sizing of an energy storage system in a direct wave energy converter," in *Proc. 9th Int. Conf. Ecol. Vehicles Renew. Energies (EVER)*, Monte-Carlo, Monaco, Mar. 2014, pp. 1–9.
[33] Y. Yang, W. Pei, W. Deng, Z. Shen, Z. Qi, and M. Zhou, "Day-ahead scheduling optimization for microgrid with battery life model," *Trans. China Electrotech. Soc.*, vol. 30, no. 22, pp. 172–180, 2015.
[34] D. B. Murray and J. G. Hayes, "Cycle testing of supercapacitors for long-life robust applications," *IEEE Trans. Power Electron.*, vol. 30, no. 5, pp. 2505–2516, May 2015.
[35] HydroWires: U.S. Department of Energy. *Energy Storage Technology and Cost Characterization Report*. Accessed: Jan. 20, 2020. [Online]. Available: https://www.energy.gov
[36] *Standard for Interconnecting Distributed Resources With Electric Power Systems*, IEEE Standard 1547, Jul. 2003.

PRANOY ROY (Graduate Student Member, IEEE) received the B.S. degree in electrical and electronics engineering from the Rajshahi University of Engineering and Technology, Bangladesh, and the M.S. degree in engineering technology from Western Carolina University, USA. He is currently pursuing the Ph.D. degree in electrical engineering with the University of Kentucky, USA, focusing on high-performance renewable energy and power electronic systems.

JIANGBIAO HE (Senior Member, IEEE) received the Ph.D. degree in electrical engineering from Marquette University, Milwaukee, WI, USA. He also worked with Eaton Corporation and Rockwell Automation before he joined GE, in 2015. He worked in industry, most recently as a Lead Engineer with GE Global Research, Niskayuna, NY, USA. He is currently an Assistant Professor of electric power area with the Department of Electrical and Computer Engineering, University of Kentucky, USA. He has authored more than 90 technical articles and ten U.S. patents in electric power area. His research interests include high-performance propulsion drives for electric transportation, renewable energies and energy storage, and fault-tolerant power conversion systems for safety-critical applications. He has served as an Editor or an Associate Editor for several prestigious journals in electric power area. He also served in the organizing committees for numerous IEEE international conferences, and has been an active member of multiple IEEE standards working groups. He was a recipient of the 2019 AWS Outstanding Young Member Achievement Award with the IEEE Industry Applications Society.

YUAN LIAO (Senior Member, IEEE) is currently a Professor with the Department of Electrical and Computer Engineering, University of Kentucky, USA. His research interests include power system protection, analysis and planning, smart grid, and renewable energy integration.